Journal of Hazardous Materials 160 (2008) 56–62

Contents lists available at ScienceDirect

Journal of Hazardous Materials

journal homepage: www.elsevier.com/locate/jhazmat

Column study of chromium(VI) adsorption from electroplating industry by coconut coir pith

Parinda Suksabye[a], Paitip Thiravetyan[b,*], Woranan Nakbanpote[c]

[a] The Joint Graduate School of Energy and Environment, King Mongkut's University of Technology Thonburi, 91 Pracha-Utit Road, Bangmod, Thungkru, Bangkok 10140, Thailand
[b] Division of Biotechnology, School of Bioresources and Technology, King Mongkut's University of Technology Thonburi, 83 Moo.8 Thakham, Bangkhuntien, Bangkok 10150, Thailand
[c] Pilot Plant Development and Training Institute, King Mongkut's University of Technology Thonburi, 83 Moo.8 Thakham, Bangkhuntien, Bangkok 10150, Thailand

ARTICLE INFO

Article history:
Received 6 February 2007
Received in revised form
27 September 2007
Accepted 26 February 2008
Available online 4 March 2008

Keywords:
Cr(VI)
Coir pith
Fixed-bed column
BDST model
Thomas model

ABSTRACT

The removal of Cr(VI) from electroplating wastewater by coir pith was investigated in a fixed-bed column. The experiments were conducted to study the effect of important parameters such as bed depth (40–60 cm) and flow rate (10–30 ml min^{-1}). At 0.05 C_t/C_0, the breakthrough volume increased as flow rate decreased or a bed depth increased due to an increase in empty bed contact time (EBCT). The bed depth service time model (BDST) fit well with the experimental data in the initial region of the breakthrough curve, while the simulation of the whole curve using non-linear regression analysis was effective using the Thomas model. The adsorption capacity estimated from the BDST model was reduced with increasing flow rate, which was 16.40 mg cm^{-3} or 137.91 mg Cr(VI) g^{-1} coir pith for the flow rates of 10 ml min^{-1} and 14.05 mg cm^{-3} or 118.20 mg Cr(VI) g^{-1} coir pith for the flow rates of 30 ml min^{-1}. At the highest bed depth (60 cm) and the lowest flow rate (10 ml min^{-1}), the maximum adsorption reached 201.47 mg Cr(VI) g^{-1} adsorbent according to the Thomas model. The column was regenerated by eluting chromium using 2 M HNO_3 after adsorption studies. The desorption of Cr(III) in each of three cycles was about 67–70%. The desorption of Cr(III) in each cycle did not reach 100% due to the fact that Cr(V) was present through the reduction of Cr(VI), and was still in coir pith, possibly bound to glucose in the cellulose part of coir pith. Therefore, the Cr(V) complex cannot be desorbed in solution. The evidence of Cr(V) signal was observed in coir pith, α-cellulose and holocellulose extracted from coir pith using electron spin resonance (ESR).

1. Introduction

Chromium has widespread use in various industries e.g. electroplating, leather tanning, textile dying and metal finishing. However, in Bangkok, Thailand, most chromium is applied to chrome-electroplating. This industry generates a high volume of Cr(VI)-contaminated wastewater (approximately 1000 m^3/day) [1]. Thus, it is necessary to treat the wastewater before being discharged into natural water.

Cr(VI) is highly toxic and ingestion results in maladies such as epigastric pain, nausea, vomiting, severe diarrhea, and hemorrhage [2]. Conventional methods have been used to remove Cr(VI) from industrial wastewater including reduction, precipitation, ion-exchange, and reverse osmosis [3,4], but these are limited by high cost excessive use of chemicals, and problems with the disposal of residual metal sludge. Adsorption by inexpensive adsorbents such as tea factory waste [5], activated eucalyptus bark [6], by-product *of Lentius* as *edodes* [7], raw rice bran [8] and lignocellulosic substrate extracted from wheat bran [2] offer a potential alternative for Cr(VI) removal.

Coconut coir pith is a waste material from the process of coir fiber separation from coconut husk for use in mattress padding. About 81,490 tons/year of coconut coir pith is generated in Prachuapkhirikhan province. In our previous research, coir pith was used as an adsorbent for the removal of Cr(VI) in batch experiments. Results show that it is effective and has a high capacity for Cr(VI) adsorption [9]. Adsorption in batch mode is not appropriate for industrial applications, however, because of a need for continuous flow of wastewater and the large volume involved. Fixed-bed columns for adsorption are simple, easy to operate and handle, regeneration capacity and sludge-free [10]. The appropriate design of a column, however, is an important factor in the dynamic removal of Cr(VI)-contaminated wastewater.

Most reported studies of Cr(VI) removal in the literature have been conducted in a batch reactor and the Cr(VI) solution is prepared from a synthetic solution [11–14]. This study was carried out to evaluate the performance of coir pith for Cr(VI) removal from actual electroplating wastewater through a fixed-bed column. The effect of parameters such as flow rate and bed depth on the shape of the breakthrough curve was investigated. The bed depth service

* Corresponding author. Tel.: +66 2 4707535; fax: +66 2 4523455.
E-mail addresses: paitip.thi@kmutt.ac.th, paitip@hotmail.com (P. Thiravetyan).

0304-3894/$ – see front matter © 2008 Elsevier B.V. All rights reserved.
doi:10.1016/j.jhazmat.2008.02.083

time (BDST) model and Thomas model were used to evaluate and predict the adsorption performance and capacity of coir pith for Cr(VI) adsorption in a fixed-bed column. Desorption and column regeneration of Cr(VI) adsorption were also investigated. The oxidation state of chromium after Cr(VI) adsorption on the coir pith was studied by electron spin resonance (ESR).

2. Materials and methods

2.1. Adsorbent preparation

Coir pith was obtained as a waste product from padding used in mattress factories, Prachuapkhirikhan province, Thailand. The coir pith in this study contained 36% lignin, 43.8% holocellulose (27.8% α-cellulose, 2.1% β-cellulose, 13.9% γ-cellulose) and 16.2% pentosan. Coir pith was dried in ambient air and then sieved through a US standard sieve with a particle size range between 150 and 1118 μm.

2.2. Electroplating wastewater

The Cr(VI)-contaminated wastewater was collected from rinse water in chrome-electroplating factory, located in Samuthprakarn province (Thailand), with a Cr(VI) concentration of 1481–1647 mg l^{-1}, pH of 1.83.

2.3. Fixed-bed column studies

The continuous flow adsorption experiment was conducted in an acrylic column consisting of two columns: each column had an internal diameter of 5 cm and a length of 35 cm. The coir pith was packed in the column between glass wool and glass beads, which prevented the wash out of coir pith. The particle size was 150–1118 μm with a bed depth of 30 cm and filling weight of 70 g in each column. The packed density or bulk density (ρ_s) of the adsorbent in the column was approximately 0.1188 g cm^{-3}. The column had three 0.5 cm (internal diameter) septa ports through which the samples were collected at time intervals using a syringe with a needle. Before operation, the bed was rinsed with distilled water and left overnight to ensure a closely packed arrangement of particles with no void, channels, or cracks. A schematic of a fixed-bed column of coir pith for Cr(V) adsorption is shown in Fig. 1. The electroplating wastewater (Cr(VI) = 1532 mg l^{-1}, pH 1.83) was fed through the fixed-bed column in an up-flow mode to avoid channelling of the effluent and compaction. The roller pump (EYELA Roller pump RP-1000) was used to control the flow rate at the inlet and outlet. The effluent samples were collected at specified time intervals and measured for the remaining Cr(VI) by a colorimetric method [15], which was spectrophotometrically analyzed (Spectronic 21, BAUSCH & LOMB) through the development of a purple–violet color with 1,5 diphenyl carbazide in acidic solution at a wavelength of 540 nm. The flow to the column was continued until the effluent Cr(VI) concentration (C_t) approached the influent Cr(VI) concentration (C_0), $C_t/C_0 = 0.97$.

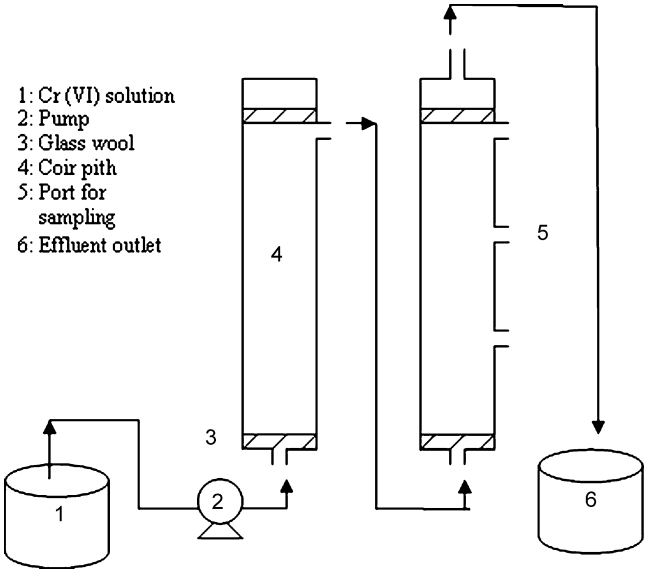

Fig. 1. A schematic of fixed-bed column of coir pith for Cr(VI) adsorption.

2.4. Effect of flow rate and bed depth

Three flow rates of 10, 20 and 30 ml min^{-1} were investigated at a constant bed depth. The studied cumulative bed depths were 40, 50 and 60 cm. The volume treated to the breakpoint and the shape of breakthrough curve for various flow rates and bed depths was compared.

2.5. Batch studies

Experiments were conducted by varying the dosage of coir pith (particle size = 150–1118 μm) in the range of 0.06–0.30 g and shaking with 10 ml of electroplating wastewater for 18 h with a system pH of 1.83 at 30 °C. The adsorbent and adsorbate were separate by centrifugation at 4500 rpm for 10 min.

2.6. Electron spin resonance (ESR) measurements

Ten milligram samples were loaded into a quartz sample tube with 5 mm diameter, and then analyzed by ESR using X-band ESR spectrometer (JEOL, JES TE-100) under the operation conditions of microwave power 5 mW, a microwave frequency 9.44 GHz, an external magnetic field of 340 mT, a field amplitude 10 mT, a field modulation 100 kHz, a modulation width 0.1 mT, a time constant 0.1 s, and sweep time of 2 min.

2.7. Desorption and column regeneration

After adsorption, the distilled water was fed through column to remove unadsorbed Cr(VI) and then followed by 2 M HNO_3 at a flow rate of 30 ml min^{-1} and bed depth of 60 cm, in order to elute the chromium. After the first regeneration, the adsorption studies were repeated. After that, the column was again regenerated and subjected to further adsorption until it could no longer adsorb chromium. In this study, the adsorption–desorption limit for Cr(VI) is three cycles. The total chromium (Cr(VI) +Cr(III)) was determined by a Inductively Coupled Plasma Spectrometer (ICP), Jobin Yvon-JY 124 France [15]. The difference in concentration between the total chromium and Cr(VI) was interpreted as the concentration of Cr(III).

3. Results and discussion

3.1. Effect of flow rate on breakthrough curves

In a previous study, Cr(VI) was shown to have a maximum adsorption percentage on coir pith at system pH of 2 because the electrostatic attraction occurring between the negatively charged $HCrO_4^-$ and the positively charged coir pith as well as the direct reduction of Cr(VI) to Cr(III) in solution [9]. For this reason, in this study, the adsorption of Cr(VI) from electroplating wastewater onto coir pith in a fixed-bed column was performed at low pH. The pH of the electroplating wastewater was 1.83. The effect of flow rate in the fixed bed of coir pith was investigated from 10 to 30 ml min^{-1}

Table 1
Parameters in fixed-bed column for chromium adsorption by coir pith (Cr(VI) = 1532 mg l^{-1}, pH 1.83, particle size 150–1118 μm)

Flow rate (ml min^{-1})	Z (cm)	Bed volume (cm^3)	t_b (h)	V_b (l)	EBCT (min)	W (g)	Usage rate (g l^{-1})
10	40	785.00	11	6.6	78.50	93.33	14.14
	50	981.25	14	8.40	98.13	116.66	13.81
	60	1177.75	18	10.8	117.75	140.00	12.96
20	40	785.00	4	4.8	39.25	93.33	19.43
	50	981.25	5.5	6.6	49.07	116.66	17.68
	60	1177.75	7.33	8.8	58.88	140.00	15.91
30	40	785.00	1.33	2.4	26.15	93.33	38.89
	50	981.25	2.50	4.5	32.71	116.66	25.81
	60	1177.75	3.33	6.0	39.25	140.00	23.33

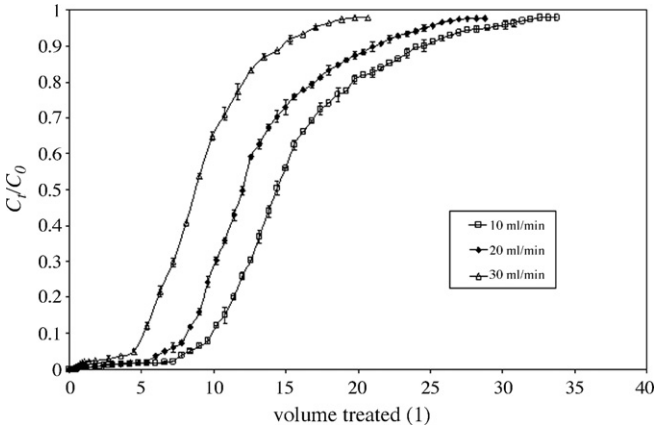

Fig. 2. Effect of various flow rates on the breakthrough curve of Cr(VI) adsorption on coir pith at 50 cm bed depth (Cr(VI) = 1532 mg l^{-1}, pH 1.83, particle size 150–1118 μm).

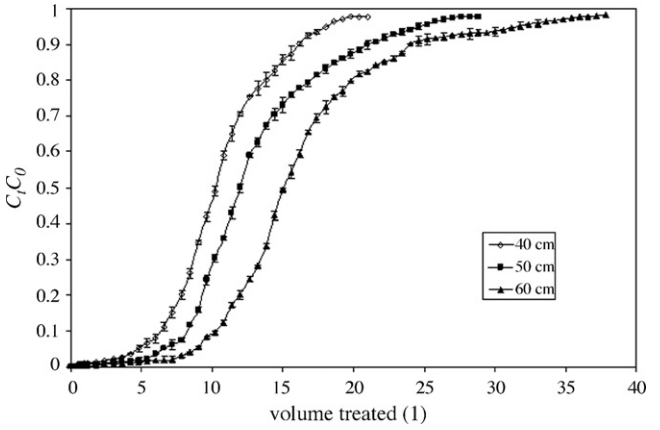

Fig. 3. Effect of various bed depth on the breakthrough curve of Cr(VI) adsorption on coir pith at flow rate 20 ml min^{-1} (Cr(VI) = 1532 mg l^{-1}, pH 1.83, particle size 150–1118 μm).

with constant bed depth. The influent Cr(VI) from electroplating wastewater in the feed was 1532 mg l^{-1}. The breakthrough curve, C_t/C_0 versus volume treated with various flow rates at a constant bed depth of 50 cm is shown in Fig. 2. When the adsorption zone moves up and the upper edge of this zone reaches the top of the column, the effluent concentration starts to rise rapidly [16]. This is called the breakthrough point. The desired breakthrough point for all flow rates was determined to be 0.05 C_t/C_0. As seen in Fig. 2, the breakthrough volume (V_b) occurred at 8.4, 6.6 and 4.5 l for flow rates of 10, 20 and 30 ml min^{-1}, respectively. The results indicate that a decrease in flow rate at constant bed depth of 50 cm increased the breakthrough volume or breakthrough time (t_b) due to an increase in empty bed contact time (EBCT), which was 98.13, 49.07 and 32.71 min for flow rates at 10, 20 and 30 ml min^{-1}, respectively (Table 1). The lower the EBCT, the less effective the diffusion process becomes, resulting in lower adsorption. Thus, the adsorbent needs more time to bond the metals efficiently [6]. The results also show that the shape of the breakthrough curve is saturated earlier at higher flow rates because the front of the adsorption zone quickly reached the top of column. In contrast, lower flow rate and longer contact time, resulted in a shallow adsorption zone.

As shown in Fig. 2, an increase in flow rate from 10 to 30 ml min^{-1} decreased the breakthrough volume from 8.4 to 4.5 l. This corresponded to a decrease in adsorption capacity from 137.91 to 118.2 mg Cr(VI) g^{-1} adsorbed (Table 2). However, the adsorption capacity of Cr(VI) on coir pith in fixed-bed column for all flow rates is high due to the fact that the surface charge of coir pith is positive ((pH 1.83 <pH_{zpc} of coir pith = 8.15), and therefore, electrostatic attraction occurred between the positively charged adsorbent and negative charged $HCrO_4^-$ [9].

For the studies on the effect of flow rate, it was suggested that lower flow rate or longer contact time would be required for Cr(VI) adsorption in the column of coir pith.

3.2. Effect of bed depth on breakthrough curves

The effect of a bed depth of 40, 50 and 60 cm on the breakthrough curve at a constant flow rate of 20 ml min^{-1} was also investigated (Fig. 3). The results show that the shape and gradient of the breakthrough curve was slightly different with the variation in bed depth. The higher uptake of Cr(VI) was observed at the beginning of the fixed-bed column, but the concentration of Cr(VI) in the effluent rapidly increased after breakthrough volume or breakthrough time. The lower bed depth gets saturated earlier than higher bed depth. As can be seen in Fig. 3, the V_b was 4.8, 6.6 and 8.8 l at bed depths of 40, 50 and 60 cm, respectively. The V_b or t_b increased when increasing the bed depth. From these results, it can be concluded that the

Table 2
Experimental constants of BDST model for Cr(VI) adsorption by coir pith (Cr(VI) = 1532 mg l^{-1}, solution pH 1.83, particte size 150–1118 μm)

Flow rate (ml min^{-1})	ν (cm h^{-1})	Slope	Intercept	N_0 (mg cm^{-3})	K (l mg^{-1} h^{-1})	R^2	Z_0 (cm)	X (mg g^{-1})
10	30.57	0.35	−3.1667	16.40	0.00060	0.9932	9.04	137.91
20	61.15	0.1667	−2.7222	15.62	0.00069	0.9967	16.71	131.36
30	91.72	0.1	−2.6111	14.05	0.00073	0.9908	26.11	118.20

increase in the Cr(VI) uptake in a column with the increase of the bed depth was due to an increase in longer contact time for Cr(VI) adsorption [17,18].

3.3. Bed depth service time (BDST) model with variation in flow rate

The BDST is a model for predicting the relationship between bed depth, Z and service time [18]. This model is used only for the description of the initial part of the breakthrough curve i.e. up to the breakpoint or 10–50% of the saturation points [6]. This BDST model was focused on the estimation of characteristic parameters such as the maximum adsorption capacity and kinetic constant. The original BDST model was carried out by Bohart and Adams and given in Eq. (1) [19]:

$$\ln\left(\frac{C_0}{C_b}-1\right)=\ln\left(\exp\left(\frac{KN_0Z}{\nu}\right)-1\right)-KC_0t \quad (1)$$

Hutchins (1973) [18] proposed a linear relationship between the bed depth and service time by rearranging as Eq. (2).

$$t_b=\frac{ZN_0}{C_0\nu}-\frac{1}{KC_0}\ln\left(\frac{C_0}{C_b}-1\right) \quad (2)$$

Where t_b is service time at breakthrough point; N_0 is adsorption capacity per volume of bed (mg cm^{-3}), Z is the depth of adsorbent bed (cm), C_0 is influent or initial solute concentration (mg l^{-1}), ν is linear flow rate (cm h^{-1}), K is rate constant of adsorption (l mg^{-1} h^{-1}) and C_b is the effluent concentration at breakthrough point (mg l^{-1}). Eq. (2) can be rewritten in the form of a straight line.

$$t_b=m_xZ-C_x \quad (3)$$

Where m_x is slope of BDST line ($m_x = N_0/C_0\nu$) and the intercept of this equation represents as Eq. (4).

$$C_x=\frac{1}{KC_0}\ln\left(\frac{C_0}{C_b}-1\right) \quad (4)$$

Thus, N_0 and K can be evaluated from slope (m_x) and the intercept (C_x) of the plot of t_b versus Z, respectively.

The critical bed depth (Z_0) is the theoretical depth of adsorbent sufficient to ensure that the outlet solute concentration does not exceed the breakthrough concentration (C_b) value at time $t = 0$. Z_0 can be calculated as Eq. (5) [6]

$$Z_0=\frac{\nu}{KN_0}\ln\left(\frac{C_0}{C_b}-1\right) \quad (5)$$

The parameters of fixed-bed column system for various flow rates and bed depths are shown in Table 1. The data indicate that the EBCT, V_b and t_b increased with decreasing flow rate or increasing bed depth.

The effect of flow rate on bed performance was studied using the BDST model. A plot of t_b versus bed depth (Z) at different flow rates is shown in Fig. 4. The equations of linear relationship were obtained with all R^2 above 0.99. This indicates the validity of the BDST model for present column system. The calculated adsorption capacity (N_0), the rate constant (K), and the critical bed depth (Z_0) are given in Table 2. It can be seen that the critical bed depth, Z_0 for the flow rate of 10, 20 and 30 ml min^{-1} should be greater than 9.04,16.71 and 26.11 cm, respectively, which represents a sufficient length of the adsorption zone to attain a satisfactory effluent [20]. The adsorption capacity was reduced from 16.40 mg cm^{-3} for flow rates of 10 ml min^{-1} to 14.05 mg cm^{-3} for flow rates of 30 ml min^{-1} (Table 2). This indicates that the adsorption capacity increased with decreasing flow rate or increasing EBCT. The amount of Cr(VI) adsorbed on coir pith (X) in unit of mg Cr(VI) g^{-1} adsorbent can be calculated by dividing N_0 with bulk

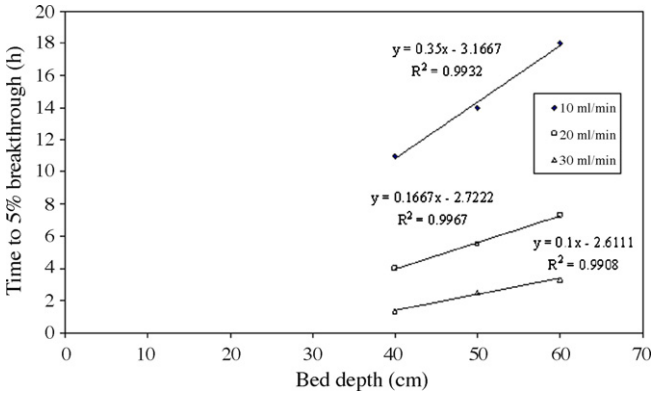

Fig. 4. BDST model at breakthrough curve in fixed-bed column for Cr(VI) adsorption by coir pith.

density (ρ_s) of coir pith in column (0.1188 g cm^{-3}). This produced 137.91, 131.36 and 118.20 mg Cr(VI) g^{-1} coir pith for flow rates of 10, 20 and 30 ml min^{-1}, respectively (Table 2). The rate constant (K) was slightly increased from 0.00060 to 0.00073 l mg^{-1} h^{-1} with increasing the flow rates from 10 to 30 ml min^{-1}.

The Cr(VI) maximum adsorption capacity (q_{max}) of coir pith sized 150–1118 μm was investigated in a batch experiment with variable dosage from 0.06 to 0.3 g at 30 °C. The q_{max} following the Langmuir model was 148 mg Cr(VI) g^{-1} adsorbent. The results indicated that the adsorption capacity of the column was lower than that of the batch system.

From the data of V_b in Table 1, the usage rate of coir pith was also determined by dividing weight of coir pith in column W with V_b [21]. It can be seen here that the usage rate of coir pith decreased with increasing EBCT.

At 50% of breakthrough, the logarithmic term in Eq. (4) reduces to zero, and the final term in the BDST equation become zero, giving the relationship as Eq. (6).

$$t_{50}=\frac{N_0}{C_0\nu}Z \quad (6)$$

If the curve of t_{50} versus Z is a straight line passing through the origin, it can be explained that the adsorption data follow the BDST model [20,22]. Fig. 5 shows the plots of the service time versus bed depth at 50% breakthrough curve. It can be seen that three straight lines nearly pass through the origin. Therefore, the data in column studies follows the BDST model.

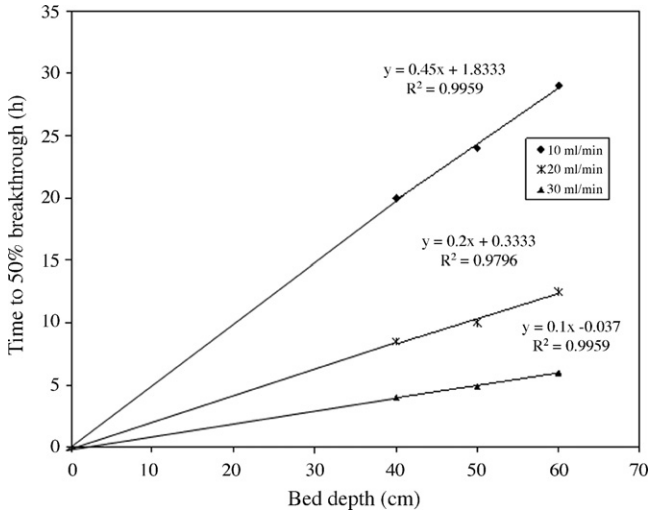

Fig. 5. BDST model at 50% breakthrough curve for Cr(VI) adsorption.

Table 3
Experimental and predicted BDST equation constants for the adsorption of Cr(VI) onto coir pith

Flow rate (ml min^{-1})	Analysis	Slope	Intercept	N_0 (mg cm^{-3})	R^2
10	Experimental	0.3500	−3.1667	16.40	0.9932
20	Experimental	0.1667	−3.1667	15.62	0.9967
20	Predicted	0.1750	−2.7222	16.40	1.0000
30	Experimental	0.1000	−3.1667	14.05	0.9908
30	Predicted	0.1166	−2.6111	16.40	1.0000

The BDST model can be extended for the prediction of a slope of the model at other flow rates. When the flow rate is changed from Q to a new value, Q', the new value of slope (m'_x) is obtained by Eq. (7). However, the intercept remains unchanged because it depends on the inlet solute concentration, C_0 [23].

$$m'_x = m_x(Q/Q') \tag{7}$$

Table 3 shows the slope and intercept of BDST equations at different flow rates predicted using a sample flow rate of 10 ml min^{-1}. It can be seen from Table 3 that the predicted and experimental values of slopes were in good agreement. The intercept is not adjusted because this term is assumed to be insignificantly affected by changing the flow rates. The advantage of the BDST model is that any experimental test can be reliably scaled up to other flow rates without further experimental runs.

The breakthrough curves predicted from BDST model were compared with the experimental breakthrough curves and the results are shown in Fig. 6. As shown, the predicted breakthrough curve fit well with the initial region of the observed breakthrough curve. There are discrepancies between the BDST predicted and experimental values above break points, however.

3.4. Application of Thomas model

The Thomas model is one of most general and widely used methods in column performance theory. The Thomas model, which assumes Langmuir kinetics of adsorption–desorption and no axial dispersion derived with the adsorption such that the rate driving force obeys second-order reversible reaction kinetics. The expression using the Thomas model for adsorption column is given as Eq. (8) [24].

$$\frac{C_t}{C_0} = \frac{1}{1 + \exp(k_{Th}/Q(q_0 x - C_0 V_{eff}))} \tag{8}$$

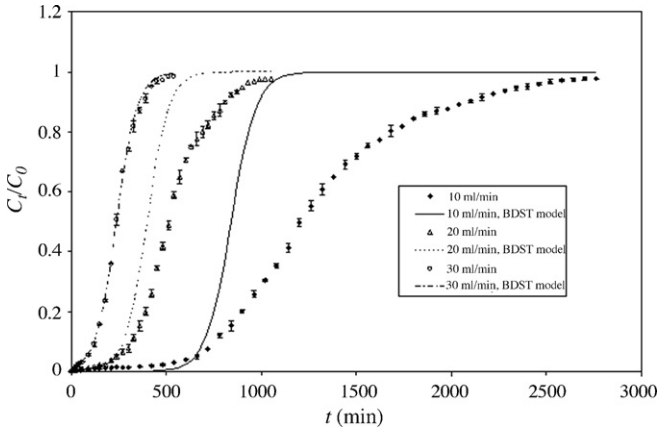

Fig. 6. Comparison of the experimental and predicted breakthrough curves obtained at different flow rates according to the BDST model (Cr(VI) = 1532 mg l^{-1}, pH 1.83, particle size 150–1118 μm, bed depth = 40 cm).

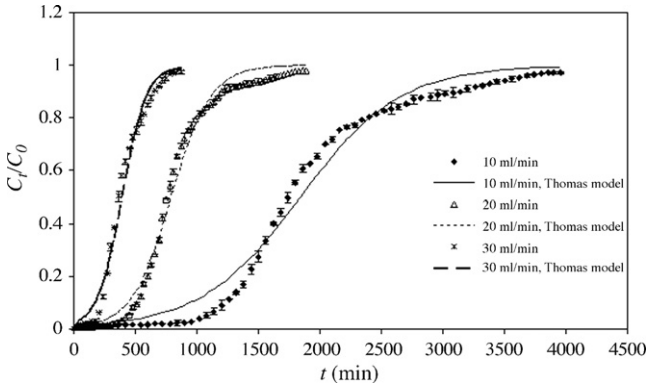

Fig. 7. Comparison of the experimental and predicted breakthrough curves obtained at different flow rates according to the Thomas model (Cr(VI) = 1532 mg l^{-1}, pH 1.83, particle size 150–1118 μm, bed depth = 60 cm).

Where k_{Th} is the Thomas rate constant (ml mg^{-1} min^{-}); q_0 is the maximum Cr(VI) adsorption per weight of adsorbent (mg g^{-1}); x is the amount of adsorbent in the column (g); V_{eff} is effluent; C_0 is the influent Cr(VI) concentration (mg l^{-1}) Q is flow rate (ml min^{-1}). C_t is the effluent Cr(VI) concentration (mg l^{-1}), t is time (min, $t = V_{eff}/Q$). The kinetic coefficient k_{Th} and the adsorption capacity of column, q_0 can be determined from a plot of C_t/C_0 against t at a given flow rate using non-linear regression.

A non-linear regression analysis of Eq. (8) was used to evaluate the Thomas model parameters of k_{Th} and q_0. The comparison of the experimental and predicted breakthrough curves obtained at different flow rates (bed depth = 60 cm) and bed depths (flow rate = 30 ml min^{-1}) according to Thomas model are shown in Fig. 7 and Fig. 8, respectively. The calculated Thomas model parameters are listed in Table 4. The results indicated that they were all acceptable fits with coefficient correlation (R^2) ranging from 0.981 to 0.996 (Table 4). As can be seen from the results, the simulation whole breakthrough curve was well predicted by the Thomas model. As seen from Table 4, at a constant bed depth of 60 cm, increasing the flow rate from 10 to 30 ml min^{-1} reduced the maximum Cr(VI) adsorption capacity from 201.47 to 128.75 mg Cr(VI) g^{-1} adsorbent while an increase in bed depth from 40 to 60 cm (constant flow rate of 30 ml min^{-1}) increased the maximum adsorption capacity, q_0, from 116.21 to 128.75 mg Cr(VI) g^{-1} adsorbent. At a bed depth of 60 cm, the rate constant, k_{Th} was

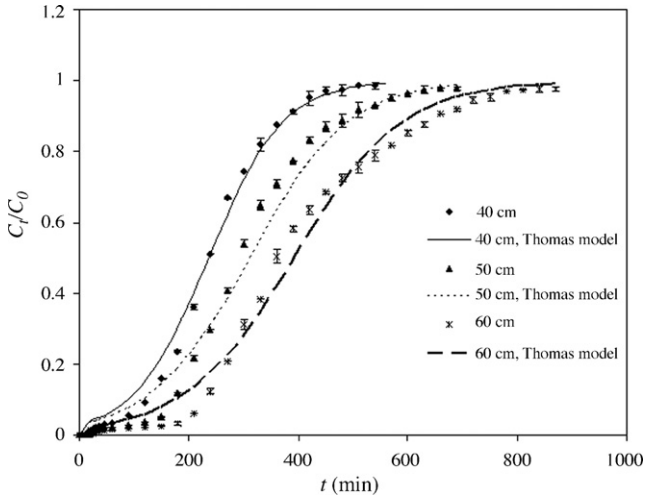

Fig. 8. Comparison of the experimental and predicted breakthrough curves obtained at different bed depth according to the Thomas model (Cr(VI) = 1532 mg l^{-1}, solution pH 1.83, particle size 150–1118 μm, flow rate = 30 ml min^{-1}).

Table 4
Thomas parameters at different condition by non linear regression analysis

Q (ml min^{-1})	Z (cm)	q_0 (mg g^{-1})	k_{Th} (ml mg^{-1} min^{-1})	R^2
10	40	196.36	0.00161	0.981
10	50	199.50	0.00205	0.990
10	60	201.47	0.00161	0.986
20	40	167.37	0.00483	0.991
20	50	172.84	0.00387	0.984
20	60	173.19	0.00409	0.993
30	40	116.21	0.00976	0.996
30	50	123.03	0.00732	0.992
30	60	128.75	0.00666	0.989

Table 5
Adsorption and desorption efficiency of chromium in multi-cycle (Cr(VI) = 1532 mg l^{-1}, solution pH l.83, particle size 150–1118 μm, bed depth = 60 cm flow rate = 30 ml min^{-1})

Cycle number	Adsorption of Cr(VI) (%)	Desorption of Cr(III) (%)
1	97.34	70.0
2	64.81	68.5
3	43.77	67.1

increased from 0.00161 to 0.00666 ml mg^{-1} min^{-1} with increasing the flow rate from 10 to 30 ml min^{-1}.

3.5. Desorption and column regeneration

When the C_t/C_0 concentration approached approximately 0.97, the adsorption process was saturated and regeneration started. In our previous batch studies, the results showed that there is very little desorption of Cr(VI) with alkaline solution (15.63% with 1 M NaOH) and desorption of Cr(VI) with acid solution (0.5–2 MHNO_3) was also unsuccessful. However, about 71.48% of Cr(III) can be desorbed by 2 M HNO_3 because most of the Cr(III) bonded on the coir pith is easily desorbed by strong acid, and some Cr(VI) bound on coir pith can be desorbed in the form of Cr(III) through reduction under strong acid conditions [9].

Therefore, in this study, 2 M HNO_3 was used as the eluent for chromium desorption. 2 M HNO_3 was passed through a column with a flow rate of 30 ml min^{-1} and a bed depth of 60 cm to regenerate the coir pith and chromium recovery. The adsorption–desorption efficiency is shown in Table 5. After desorption or regeneration was completed, the coir pith was used again in a subsequent adsorption experiment. As can be seen from Table 5, it was observed that the efficiency of Cr(VI) adsorption on regenerated coir pith in the second cycle (64.81%) and the third cycle (43.77%) dropped from the first cycles (original coir pith). In addition, the desorption of Cr(III) in three cycles is about 67–70%. Thus, the efficiency of Cr(VI) adsorption using regenerated coir pith was reduced and the desorption of Cr(III) in each cycle fails to reach 100%. This suggested that the other form of chromium was still in the coir pith. ESR was used to investigate the oxidation state of chromium adsorbed on the coir pith after Cr(VI) adsorption. ESR signals of Cr(V) and Cr(III) were observed in coir pith (Fig. 9). In addition, the ESR signal of Cr(V) obtained by the reduction of Cr(VI) was present in α-cellulose and holocellulose extracted from coir pith (Fig. 9). This suggested that the Cr(V) may be bound with glucose composing in cellulose part of coir pith. Therefore, the Cr(V) complex cannot be desorbed in the solution.

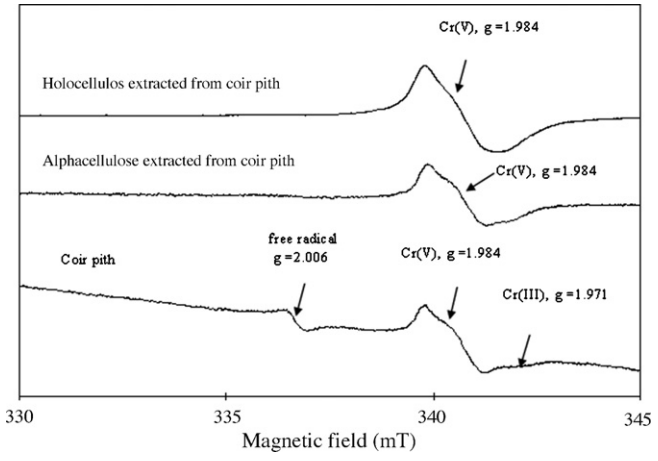

Fig. 9. Electron spin resonance spectra of coir pith, α-cellulose, holocelluose extracted from coir pith adsorbed Cr(VI) from electroplating wastewater.

4. Conclusions

The low cost coir pith has a potential as an adsorbent to remove the Cr(VI). The Cr(VI) adsorption method by coir pith had an advantage compared to the conventional method due to metal regeneration. Among available conventional process used to remove Cr(VI), most commonly used are reduction and precipitation as chromium hydroxide, but these methods have the problems in the disposal of the residual metal sludge.

Coir pith is an effective adsorbent for Cr(VI) removal through a fixed-bed column. Cr(VI) adsorption through fixed-bed columns is dependent on the flow rate and bed depth. The breakthrough volume (V_b) increased with decreasing flow rate and increasing bed depth due to an increase the EBCT. The BDST was used to evaluate the column capacity. At the breakthrough point of 0.05 C_t/C_0, the data followed the BDST model, and the adsorption capacity was decreased with increasing flow rate, which was 16.40 mg cm^{-3} or 137.91 mg Cr(VI) g^{-1} coir pith for the flow rate of 10 ml min^{-1} and 14.05 mg cm^{-3} or 118.2 mg Cr(VI) g^{-1} coir pith for the flow rate of 30 ml min^{-1}. The BDST model plot at 10 ml min^{-1} was used to predict bed depth-service time data at different flow rates. The BDST model predicted values always coincide with experimental values. The BDST fit well with the experimental data in the initial region of breakthrough curve, while the simulation of the whole breakthrough curve using non-linear regression for analysis was effective with use of the Thomas model. At the highest bed depth (60 cm), and the lowest flow rate (10 ml min^{-1}), the maximum adsorption reached 201.47 mg Cr(VI) g^{-1} adsorbent according to the Thomas model. After the adsorption process was saturated and regeneration started. The desorption of Cr(III) by 2 M HNO_3 in three cycles was about 67–70%. This suggested that the other form of chromium was still in the coir pith. Furthermore, ESR signal of Cr(V) revealed in coir pith, α-cellulose and holocellulose extracted from coir pith. These suggested that Cr(V) may be bound with glucose composing in cellulose part of coir pith. Therefore, the Cr(V) complex cannot be desorbed in solution by strong acid.

Acknowledgement

The authors gratefully acknowledge the Commission of Higher Education for providing the research funds.

References

[1] N. Kungsricharoern, Application of electrochemical precipitation of treatment of Cr wastewater, Thesis, Asian Institute of Technology, Bangkok, 1994.
[2] L. Dupont, E. Guillon, Removal of hexavalent chromium with a lignocellulosic substrate extracted from wheat bran, Environ. Sci. Technol. 37 (2003) 4235–4241.
[3] Y.C. Sharma, Cr(VI) removal from industrial effluents by adsorption on an indigenous low cost material, Colloid Surf. A: Physiochem. Eng. Aspects 215 (2003) 155–162.

[4] M. Kobya, Removal of Cr(VI) from aqueous solutions by adsorption onto hazelnut shell activated carbon: kinetic and equilibrium studies, Bioresour. Technol. 91 (2004) 317–321.
[5] E. Malkoc, Y. Nuhoglu, Fixed bed studies for the sorption of chromium(VI) onto tea factory waste, Chem. Eng. Sci. 61 (2006) 4363–4372.
[6] V. Sarin, T.S. Singh, K.K. Pant, Thermodynamic and breakthrough column studies for the selective sorption of chromium from industrial effluent on activated eucalyptus bark, Bioresour. Technol. 97 (2006) 1986–1993.
[7] G.Q. Chen, G.M. Zeng, X. Tu, C.G. Niu, G.H. Huang, W. Jiang, Application of a by-product *of Lentinus edodes* to the bioremediation of chromate contaminated water, J. Hazard. Mater. B135 (2006) 249–255.
[8] E.A. Oliveira, S.F. Montanher, A.D. Andrade, J.A. Nobrega, M.C. Rollemberg, Equilibrium studies for the sorption of chromium and nickel from aqueous solutions using raw rice bran, Process Biochem. 40 (2005) 3485–3490.
[9] P. Suksabye, P. Thiravetyan, W. Nakbanpote, S. Chayabuta, Chromium removal form electroplating wastewater by coir pith, J. Hazard. Mater. 141 (2007) 637–644.
[10] S. Kundu, A.K. Gupta, and modelling of fixed bed column operation on As (V) removal by adsorption onto iron oxide-coated cement (IOCC), J. Colloid Interface Sci. 290 (2005) 52–60.
[11] G. Arslan, E. Pehlivan, Batch removal of chromium(VI) from aqueous solution by Turkish brown coals, Bioresour. Technol. 98 (2007) 2836–2845.
[12] S. Babel, T.A. Kurniawan, Cr(VI) removal from synthetic wastewater using coconut shell charcoal and commercial activated carbon modified with oxidizing agents and/or chitosan, Chemosphere 54 (2004) 951–967.
[13] G.S. Agarwal, H.K. Bhuptawat, S. Chaudhari, Biosorption of aqueous chromium(VI) by *Tamarindus indica* seeds, Bioresour. Technol. 97 (2006) 949–956.
[14] S. Deng, R. Bai, Removal of trivalent and hexavalent chromium with aminated polyacrylonitrile fibers: performance and mechanisms, Water Res. 38 (2004) 2423–2431.
[15] American Public Health Association (APHA), American Water Works Association (AWWA), Water Environment Federation (WEF), Standard Methods for the examination of water and wastewater, 20th ed. American Public Health Association Press, Washington, 1998.
[16] S.D. Faust, O.M. Aly, Adsorption Process for Water Treatment, Butterworths, Boston, 1987.
[17] S. Kundu, A.K. Gupta, As (III) removal from aqueous medium in fixed bed using iron oxide-coated cement (IOCC): experimental and modeling studies, Chem. Eng. J. 122 (2006) 93–106.
[18] K. Vijayaraghavan, D. Prabu, Potential of *Sargassum wightii* biomass for copper(II) removal from aqueous solution: application of different mathematic models to batch and continuous biosorption data, J. Hazard. Mater. B137 (2006) 558–564.
[19] T.S. Singh, K.K. Pant, Experimental and modelling studies on fixed bed adsorption of As(III) ions from aqueous solution, Sep. Purif. Technol. 48 (2006) 288–298.
[20] S. Netpradith, P. Thiravetyan, S. Towprayoon, Evaluation of metal hydroxide sludge for reactive dye adsorption in a fixed-bed column system, Water Res. 38 (2004) 71–78.
[21] W.W. Eckenfelder, Adsorption, in: Industrial Water Pollution Control, 3rd ed., McGraw-Hill International, Boston, 2000.
[22] Z. Zulfadhly, M.D. Mashitan, S. Bhatia, Heavy metals removal in fixed bed column by macro fungus *Pycnoporus sanguineus*, Environ. Pollut. 112 (2001) 463–470.
[23] V.C. Taty-Costodes, H. Fauduet, C. Porte, Y.S. Ho, Removal of lead (II) ions from sysnthetic and real effluents using immobilized *Pinus Sylvestris* sawdust: adsorption on a fixed-bed column, J. Hazard. Mater. B123 (2005) 135–144.
[24] Z. Aksu, F. Gonen, Biosorption of phenol by immobilized activated sludge in a continuous pack bed: prediction of breakthrough curves, Process Biochem. 39 (2004) 599–613.